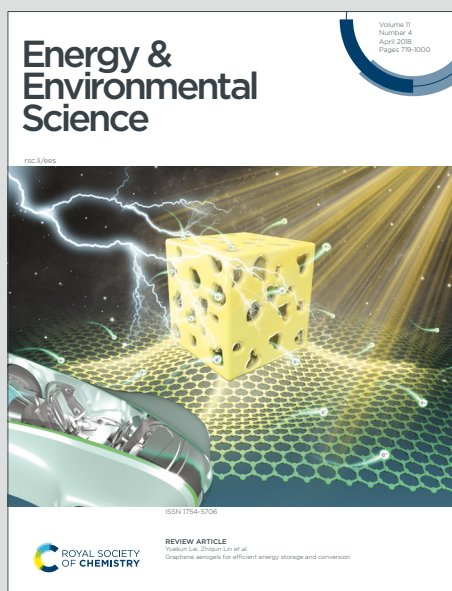


Energy & Environmental Science

Accepted Manuscript

This article can be cited before page numbers have been issued, to do this please use: G. Studer, A. Schmidt, J. Büttner, M. Schmidt, A. Fischer, I. Krossing and B. Esser, *Energy Environ. Sci.*, 2023, DOI: 10.1039/D3EE00235G.



This is an Accepted Manuscript, which has been through the Royal Society of Chemistry peer review process and has been accepted for publication.

Accepted Manuscripts are published online shortly after acceptance, before technical editing, formatting and proof reading. Using this free service, authors can make their results available to the community, in citable form, before we publish the edited article. We will replace this Accepted Manuscript with the edited and formatted Advance Article as soon as it is available.

You can find more information about Accepted Manuscripts in the [Information for Authors](#).

Please note that technical editing may introduce minor changes to the text and/or graphics, which may alter content. The journal's standard [Terms & Conditions](#) and the [Ethical guidelines](#) still apply. In no event shall the Royal Society of Chemistry be held responsible for any errors or omissions in this Accepted Manuscript or any consequences arising from the use of any information it contains.

Broader context statement:

Due to the scarcity of lithium and transition metal oxides used in traditional batteries, there is a strong impetus to develop alternative battery technologies for applications ranging from small devices to large scale stationary storage of electricity. Since aluminium is one of the most widely available elements in the Earth's crust, Al-based batteries are considered promising candidates for such next-generation energy storage solutions. However, to date it remains a challenge to identify appropriate host electrode materials that reversibly insert (complex) aluminium ions. In this article we demonstrate a strategy for designing such positive electrode materials. This strategy involves using an organic redox polymer as positive electrode material, which reversibly inserts two $[\text{AlCl}_4]^-$ ions with a specific capacity that surpasses that of graphite as positive electrode material. In addition, it shows a superior cyclability at fast C-rates. This concept could pave the way towards the development of advanced Al-based batteries and affordable energy storage solutions.



ARTICLE

On a high-capacity aluminium battery with a two-electron phenothiazine redox polymer as positive electrode

Gauthier Studer,^{a,b} Alexei Schmidt,^{b,c} Jan Büttner,^{b,c,d} Maximilian Schmidt,^a Anna Fischer,^{b,c,d} Ingo Krossing,^{*b,c,d} Birgit Esser^{*a,b,d}Received 00th January 20xx,
Accepted 00th January 20xx

DOI: 10.1039/x0xx00000x

With aluminium being the most abundant metal in Earth's crust, rechargeable Al ion batteries (AIBs) hold great promise as next-generation energy storage devices. However, today's positive electrode materials for AIBs suffer from low available specific capacities, which limits the specific energies of published AIBs. Here, we present an organic redox polymer with two well-defined redox processes as a positive electrode material that overcomes these shortcomings. Cross-linked poly(3-vinyl-*N*-methylphenothiazine) with phenothiazine as two-electron redox centre reversibly inserts $[\text{AlCl}_4]^-$ ions at potentials of 0.81 and 1.65 V vs. $\text{Al}|\text{Al}^{3+}$, delivers in AIBs experimental specific capacities of up to 167 mAh g^{-1} and surpasses graphite as positive electrode material. After 5,000 cycles at a 10 C rate this AIB retains 88% of its capacity. Even at a 100 C rate, 64 mAh g^{-1} can be reversibly cycled, and the AIB returns unchanged to its original capacities at slower rates. This is the first report of a reversible two-electron redox process for a phenothiazine-based battery electrode material. With its high discharge voltage and specific capacity, its excellent capacity retention at fast C-rates combined with flat charge/discharge plateaus, this AIB constitutes a major advance in the development of rechargeable AIBs and will initiate further explorations of organic redox polymers as positive electrode materials, paving the way towards more sustainable energy storage solutions.

Introduction

Climate change and the increasing demand for electrical energy require the development of novel types of devices for the storage of renewable energy. While classical lithium-ion batteries^{1,2} might profit from engineered electrode materials,^{3–5} next-generation batteries^{6,7} should rely on abundant elements, be safe and of low cost, use non-toxic materials and be easy to recycle. With 8.1 wt%, aluminium is the most abundant metal in the Earth's crust and its recycling is easy.⁸ With its very high volumetric capacity of 8040 mAh cm^{-3} as negative electrode material, Al even exceeds that of lithium of 2046 mAh cm^{-3} .⁹ By contrast to the latter, it can be reversibly stripped and deposited without forming dendrites,^{7,10} preventing short circuits. Favourably, the ionic liquid electrolytes currently used in Al batteries are non-flammable.¹¹ Hence, rechargeable Al ion batteries (AIBs) hold great promise as storage devices.^{9,12,13} Yet, the development of rechargeable AIBs faces fundamental

challenges and in particular lacks suitable positive electrode materials, leaving them still in their infancy.^{14–16}

Two types of charge storage mechanism for positive electrodes are known for the Al(III) species formed upon cycling: Storage as cationic (Al^{3+} , $[\text{AlCl}]^{2+}$, $[\text{AlCl}_2]^+$) or anionic ($[\text{AlCl}_4]^-$, $[\text{Al}_2\text{Cl}_7]^-$) (complex) aluminium ions. Only few examples have been reported where Al^{3+} ions were reversibly stored, probably due to their high charge density and low mobility.^{17–19} In some cases monocationic $[\text{AlCl}_2]^+$ ions^{20,21} or dicationic $[\text{AlCl}]^{2+}$ ions^{22–24} with reduced charge densities were stored. Therefore, the more favourable anion insertion mechanism is the main approach currently taken. It proceeds with high reversibility, enabling fast charge/discharge rates and large operating potentials. The most studied positive electrode material (PEM) for $[\text{AlCl}_4]^-$ storage is graphite, following the seminal report by Lin et al. in 2015.²⁵ Al/graphite cells typically show a flat discharge potential of 1.8–1.9 V vs. $\text{Al}|\text{Al}^{3+}$, good rate capability and cycling stability.²⁶ However, the specific discharge capacities of graphite are limited to ca. 120 mAh g^{-1} , with few reports on higher values, and specific energies⁵ of up to 69 Wh kg^{-1} .^{27–29}

Organic PEMs are excellent candidates for $[\text{AlCl}_4]^-$ insertion, potentially enabling higher capacities and energy densities.³⁰ Many p-type organic compounds can be reversibly oxidized at high potentials (up to 4 V vs. $\text{Li}|\text{Li}^+$) and thereby store and release anions at fast charge/discharge rates.³¹ Organic PEMs were predominantly explored in Li-organic cells,^{32,33} but there are a few examples where p-type organics were used as PEMs in AIBs:^{34–36} The conductive polymers polypyrrole and polythiophene³⁷ were first investigated and provided specific capacities of 30–100 mAh g^{-1} as well as specific energies⁵ of

^a Institute of Organic Chemistry II and Advanced Materials, Albert-Einstein-Allee 11, 89081 Ulm, Germany; Email: birgit.esser@uni-ulm.de; www.esserlab.com

^b Freiburg Materials Research Centre, University of Freiburg, Stefan-Meier-Str. 21, 79104 Freiburg, Germany; Email: krossing@uni-freiburg.de

^c University of Freiburg, Institute of Inorganic and Analytical Chemistry, Albertstraße 21, 79104 Freiburg, Germany; www.krossing-group.de

^d Cluster of Excellence livMatS @ FIT – Freiburg Centre for Interactive Materials and Bioinspired Technologies, University of Freiburg, Georges-Köhler-Allee 105, 79110 Freiburg, Germany

Electronic Supplementary Information (ESI) available: [details of any supplementary information available should be included here]. See DOI: 10.1039/x0xx00000x



around 45 Wh kg⁻¹. Polypyrenes³⁸ showed slightly better performance with an average capacity of 100 mAh g⁻¹ at 1.6–2.0 V vs. Al|Al³⁺ discharge voltage, while poly(3,4-ethylenedioxythiophene) (PEDOT)³⁹ gave energy densities⁵ of 50–64 Wh kg⁻¹ at a lower average discharge potential of 1.3 V. Recently, polymeric triarylamine were investigated, polymerized *in situ* within the electrode during electrochemical cycling from small molecule triarylamine precursors.⁴⁰ A reversible capacity of 135 mAh g⁻¹ was demonstrated, but with sloppy charge/discharge profiles around an average voltage of 1.1 V vs. Al|Al³⁺, resulting from the ill-defined structure of the organic PEM. A similar approach was taken in another recent report on aminopyrenes, which were oligomerized *in situ* and showed specific discharge capacities of up to 195 mAh g⁻¹ within a potential range of 0.1–2.2 V vs. Al|Al³⁺, but also associated with sloppy charge/discharge profiles.⁴¹ The performance of pyrenes could recently be boosted through combination with dihydrophenazines in conjugated microporous polymers, furnishing attractive capacities exceeding 200 mAh g⁻¹ at potentials of 0.5 and 1.5 V vs. Al|Al³⁺.⁴²

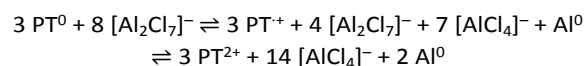
By contrast, (aliphatic) redox polymers are ideal candidates as organic PEMs:⁴³ As opposed to conductive polymers they contain electronically separated redox centres, resulting in well-defined redox processes, and their incorporation into a (cross-linked) polymer backbone renders them insoluble in battery electrolytes. Phenothiazine (PT) is a particularly well-suited p-type redox-active group, as it can undergo two reversible oxidations to a dication at relatively high redox potentials of 3.6 and 4.1 V vs. Li|Li⁺. PT-based polymers have shown excellent performance in Li-organic cells, regarding cycling stability and rate capability.^{44–48} Limiting their capacity, however, only the first redox process of each PT unit could be reversibly addressed in cells with LiPF₆/carbonate-based electrolytes, which resulted in only lower (reversible) specific capacities of up to 112 mAh g⁻¹ for poly(3-vinyl-*N*-methylphenothiazine) (PVMPT)⁴⁴ or its cross-linked derivative X-PVMPT.⁴⁶ Possibly the PT dications undergo irreversible side reactions with the carbonate-based electrolyte molecules, rendering the second redox process irreversible.

Herein, we investigated cross-linked poly(3-vinyl-*N*-methylphenothiazine) (X-PVMPT) as PEM in AIBs with a 1-ethyl-3-methylimidazolium (EMIm)-based chloroaluminate ionic liquid electrolyte. In this medium, both redox processes of each PT unit can be reversibly addressed (Fig. 1a). Notably, this is the first report of a reversible two-electron redox process for any phenothiazine-based battery electrode material.⁴⁹ Hence, each PT unit in X-PVMPT can be oxidized from its neutral state **A** over the radical cation state **C** to the dication state **D**. In the intermediate oxidation state **B**, π*–π*–interactions between neutral and oxidized PT units evolve.⁴⁷ This is relevant for the Al|X-PVMPT battery, as will be discussed below. X-PVMPT-based electrodes insert [AlCl₄]⁻ or [Al₂Cl₇]⁻ ions at average charge potentials of 0.81 and 1.65 V vs. Al|Al³⁺ with high reversibility and at fast charge/discharge rates. Experimental specific capacities of up to 167 mAh g⁻¹ are accessible (theor.: 221 mAh g⁻¹). Thus, the electrodes clearly surpass graphite as PEM. Very recently, a phenoxazine-based polymer was reported

as PEM for Al batteries, featuring with up to 133 mAh g⁻¹ lower discharge capacities than X-PVMPT.⁵⁰ In addition, the X-PVMPT-based electrodes show an excellent cycling stability, where 5,000 cycles at 10 C rate proceed with 88% retention of the initial specific capacity. The redox processes are well distinguishable with a small voltage hysteresis between charge and discharge, even at high C-rates. This is a major advance compared to other reported organic PEMs for AIBs.

Results and discussion

Each phenothiazine unit in the polymer X-PVMPT can undergo a two-electron oxidation from the neutral state **A** to a dication **D** via the radical cation state **C** (Fig. 1a). This can be seen in cyclic voltammograms (CVs) of the non-crosslinked polymer PVMPT in solution⁴⁷ and was further confirmed by DFT calculations (see ESI for details). In isolated *N*-methylphenothiazine (MPT) as the redox-active subunit in X-PVMPT the calculated potential difference between the first redox process (**A** → **C**) and the second redox process (**C** → **D**) amounts to 1.22 V. In the polymer X-PVMPT, cation–π*–π*–interactions lead to a stabilization of the oxidized states and the occurrence of an intermediate oxidation state **B**, in which only every other PT unit is oxidized to a radical cation (Fig. 1a).⁴⁷ For the DFT calculations, we used a dimeric subunit of the polymer as reference compound (MPT-dimer, see ESI for details). The occurrence of state **B** leads to a shift in the calculated redox potentials and a smaller potential difference between the two redox processes (oxidation states **C** and **D**) of only 0.64 V compared to MPT. This calculated potential difference correlates well with that measured in the CV in the Al|X-PVMPT cells of 0.76 V (e.g. in cycle 20, see Fig. 2a below). A scheme of the Al|X-PVMPT battery is shown in Fig. 1b. In the Al|X-PVMPT cells, the room temperature ionic liquid, EMIm chloride with 1.5 added equivalents of AlCl₃ (AlCl₃ : [EMIm]Cl = 1.5 : 1), served as electrolyte. Due to its wide electrochemical window, good ionic conductivity and relatively low viscosity, EMIm-chloroaluminates are the most used electrolytes in non-aqueous AIBs.¹² Excess AlCl₃ is required to form [Al₂Cl₇]⁻ from [AlCl₄]⁻, and both complex anions are needed for reversible Al plating and stripping on the negative electrode.^{51–53} The overall stoichiometry of the electrochemical reaction in the AIB is the following (PT indicates one redox-active phenothiazine subunit of X-PVMPT):



Here, PT⁰ corresponds to oxidation state **A** in Fig. 1a, PT⁺ to state **C** and PT²⁺ to oxidation state **D**. Since we use a larger excess of electrolyte vs. the amount of counterions needed for PT^{0/+2+}, both anions [AlCl₄]⁻ and [Al₂Cl₇]⁻ are available to insert for charge balancing in the positive electrode. From size arguments, one may suggest that the smaller [AlCl₄]⁻ anion (ionic radius of 3.2 Å) may have a higher share (ionic radius of 5–6 Å).⁵⁴



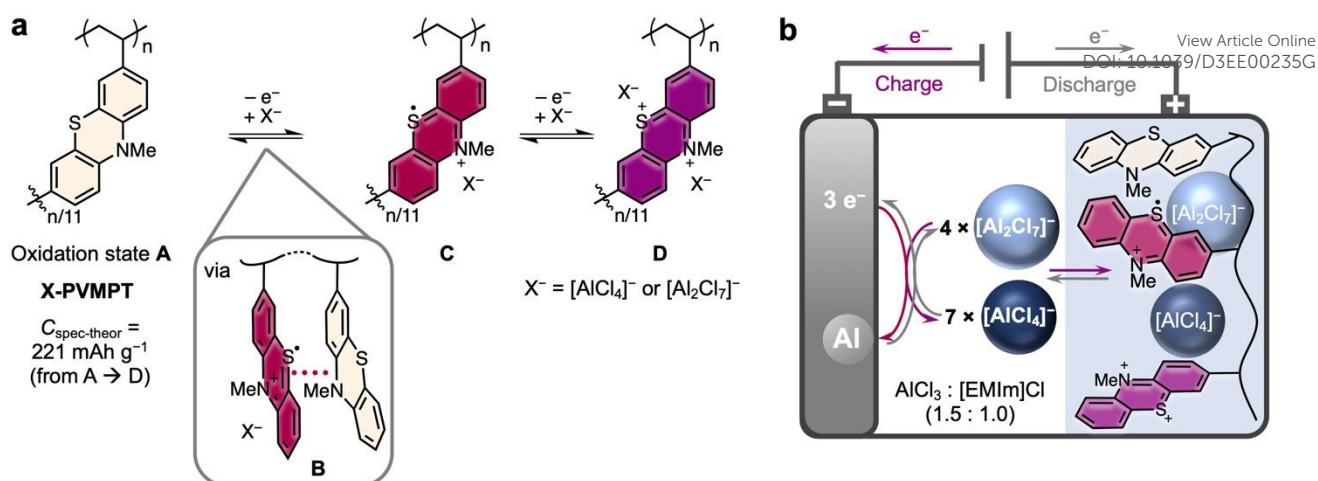


Fig. 1 | Concept of the Al/X-PVMPT battery. a, Redox processes in phenothiazine-based polymer X-PVMPT with oxidation states A, B, C and D. b, Schematic setup of the Al/X-PVMPT battery (the colours of the redox states of the PT units were chosen similarly to those experimentally observed).

Recently, benzene was shown to be an additive that reduces the viscosity of this electrolyte, yet maintains its ability to reversibly deposit Al.⁵⁵ We reasoned that the more polar fluorinated benzenes with strong sp²-C-F bonds could be superior candidates as additives due to their higher polarity but maintained stability towards Lewis-acid-induced side reactions. Hence, we investigated fluorobenzene, 1,2-difluorobenzene, 1,2,3-trifluorobenzene, 1,2,3,4-tetrafluorobenzene, pentafluorobenzene, and hexafluorobenzene as additives. However, compared to the pristine AlCl₃ : [EMIm]Cl (1.5 : 1) electrolyte, adding the fluorinated benzenes did not lead to a significant improvement. In some cases, slightly lower overpotentials for Al deposition were observed, but this effect was minor, and we therefore proceeded using the pristine electrolyte (see Supplementary Information, section 1 with Figures S1–S10 for details).

Electrochemical performance

To evaluate the electrochemical performance of X-PVMPT in AIBs, composite electrodes were fabricated containing 50 wt% X-PVMPT, 45 wt% acetylene black as conductive additive and 5 wt% PVDF as binder on molybdenum discs as current collector (Figure S14 shows the electrochemical stability window of the Mo current collector). Metallic Al was used as the counter and reference electrode, and electrochemical measurements were performed in Swagelok-type cells (Figure S13). We optimized the potential range to 0.30–2.20 V vs. Al|Al³⁺ to obtain the maximum capacity from X-PVMPT as active electrode material, but avoid the partially irreversible and slower insertion and adsorption of chloroaluminate anions on the carbon additive (see ESI for details, Figures S15–S17). Measurements using only acetylene black on molybdenum current collector at similar current density as applied to the X-PVMPT electrodes at 10 C rate cycling (3.1 mA cm⁻²) showed less than 10 mAh g⁻¹ of specific charge and discharge capacity (Figures S18 and S19), confirming that only X-PVMPT showed significant

electrochemical activity in the investigated potential range of 0.30–2.20 V vs. Al|Al³⁺.

The CVs of the first 20 cycles of an Al/X-PVMPT cell at 0.2 mV s⁻¹ (Fig. 2a) show two well separated redox processes, which correspond to the two oxidations of each PT unit in the polymer X-PVMPT (A to C and C to D, see Fig. 1a). The first redox process is centred at $E_{1/2} = 0.79$ V vs. Al|Al³⁺ and characterized by a small peak-to-peak separation of 91 mV. This underlines the reversibility and faradaic nature of this redox event. Between cycle 1 and 20 the potential remains constant. The second redox process, on the other hand, shows a gradual change over the first 20 cycles. In anodic (oxidative) scan direction, the peak potential in the first cycle appears at 1.91 V vs. Al|Al³⁺ and in further cycles is split into two peaks with peak potentials of 1.58 and 1.84 V vs. Al|Al³⁺. In cathodic (reductive) scan direction, the peak potential for the second redox event remains constant over 20 cycles at 1.52 V vs. Al|Al³⁺. This change in the anodic scan direction indicates an activation process occurring in the PEM, which might be related to rearrangement processes within the polymer, allowing for stabilizing cation-π*–π*–interactions between PT units to form and the occurrence of the intermediate oxidation state B (Fig. 1a).⁴⁷ This results in a stabilization and therefore decrease in redox potential of the second oxidation step over the initial cycles (from $E_{1/2} = 1.88$ V to $E_{1/2} = 1.55$ V vs. Al|Al³⁺), furnishing a final potential difference of 0.76 V between the two redox waves. We also observed this activation process in galvanostatic measurements, where only after a preconditioning period with 50 cycles at 0.5 C the maximum performance of the X-PVMPT electrodes was obtained (see Figure S20). The differential capacity plots of the pre-conditioning cycles show a profile similar to the CVs from Fig. 2a, where the second redox process (oxidation state C to D, see Fig. 1) is also split into two peaks initially, but merges into one peak after ca. 20 cycles, see Figures S21 and S22). Such pre-cycling has also been reported to be required for other AIBs.⁵⁶



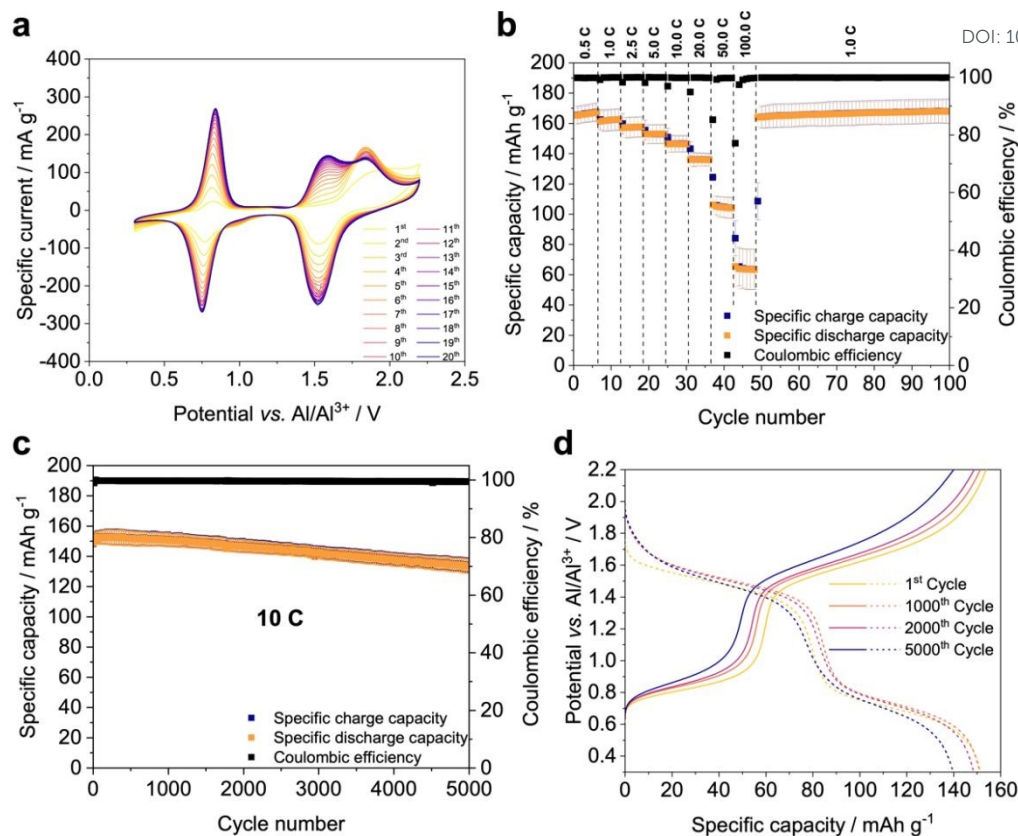


Fig. 2 | Electrochemical performance of Al/X-PVMPT batteries. a, Cyclic voltammograms of X-PVMPT-based electrodes vs. Al, first 20 cycles (0.2 mV s^{-1}). b, Constant current cycling at varying C-rates, average over three cells with error bars ($0.5 \text{ C} = 0.16 \text{ mA cm}^{-2}$, $100 \text{ C} = 31 \text{ mA cm}^{-2}$). * c, Constant current cycling at 10 C rate (3.1 mA cm^{-2}), average over three cells with error bars. * d, Charge/discharge profiles of selected cycles from plot c at 10 C rate. (*after 50 cycles of pre-conditioning at 0.5 C rate).

Fig. 2b shows the constant current cycling data of Al/X-PVMPT cells at different C-rates (average of three cells shown) after 50 cycles of pre-conditioning at 0.5 C rate. At a 0.5 C rate, equivalent to a current density of 0.16 mA cm^{-2} or 0.11 A g^{-1} of active material, a high average specific discharge capacity of 167 mAh g^{-1} was accessible. This corresponds to 76% of the theory (221 mAh g^{-1}) and shows that most of the PT-units in X-PVMPT participate in the two consecutive reversible redox processes (cf. Fig. 1a). Such reversible behaviour for the two redox reactions of each PT unit was never reported before.⁴⁹ We assume that the discrepancy between theoretical and experimentally accessible specific capacity is related to the occurrence of oxidation state **B** (see Fig. 1a) as the discharged form of the polymer, based on previous studies on PVMPT in Li-based half cells^{47,57} and on our SEM/EDX studies discussed below. In state **B**, every other PT unit is still in its radical cation form, which means that only 1.5 electrons are transferred per PT unit during discharge, and consecutively in all following charge/discharge cycles. This corresponds well with the observation that 76% of the theoretical specific capacity are accessible in the experiment, assuming that cycling occurs between oxidation states **B** and **D**, and also with the fact that the plateau at lower potential corresponding to the oxidation from **B** to **C** is associated with a smaller capacity than the plateau at higher potential, corresponding to the oxidation from **C** to **D** (Fig. 2d).

The X-PVMPT-based electrodes showed excellent rate performance. Even at a high 20 C rate, corresponding to current densities of 6.2 mA cm^{-2} and 4.4 A g^{-1} of active material, the reversible specific discharge capacities amount to record-breaking 136 mAh g^{-1} (see comparative Table S7 in the ESI).^{30,58,59} At 50 and 100 C (11 and 22 A g^{-1} , respectively), the specific discharge capacities declined more strongly, but still reached respectable average values of 105 and 64 mAh g^{-1} , respectively. Reducing the current to a 1 C rate refurbished the initial specific capacity and allowed stable cycling for a further 50 cycles at an average capacity of 166 mAh g^{-1} , which demonstrates that no decomposition of the active material took place, even at rates as high as 100 C . The decline in specific capacity at rates above 20 C may result from several factors: From the differential capacity plots (Figure S23) it follows that the two redox processes of X-PVMPT are centred at 0.80 and $1.55 \text{ V vs. Al|Al}^{3+}$ at a slow 0.5 C rate with small peak-to-peak separation of 48 mV and 47 mV , respectively. These values do not significantly change up to a rate of 20 C . Starting from 50 C , however, the battery experiences a greater polarization with 307 mV and 256 mV peak separation for the two redox processes and increased ohmic losses resulting from the internal resistance of the cell. This can cause the cell to prematurely reach the pre-defined cutoff potential before the active material has completed the electrochemical process, as is well visible in the charge/discharge curves in Figure S24. These



overpotentials at high C-rates can be rationalized by a lack of electronic conductivity of **X-PVMPT** as aliphatic polymer and by limitations in ion transport processes at very high rates.³¹

The specific energies of the Al/**X-PVMPT** cells, taking into account the masses of active materials in electrodes and electrolyte, reach up to 30 Wh kg⁻¹, but particularly impressive are the power densities of up to 7,000 W kg⁻¹, clearly surpassing those of Al/graphite batteries (see section 2.3 in the Supplementary Information and Figure S35).^{28,29,60}

We next investigated the long-term cycling performance of Al/**X-PVMPT** cells at a high 10 C rate – equal to a current density of 3.1 mA cm⁻² or 2.2 A g⁻¹ of active material (Fig. 2c). An average of three cells was measured, demonstrating the reproducibility of the obtained data (for individual plots see Figure S25). From the initial average specific discharge capacity of 151 mAh g⁻¹, 88% were retained after 5,000 cycles at 10 C rate. This corresponds to a capacity fade of only 0.0024% per cycle, demonstrating an excellent long-term cycling stability of the Al/**X-PVMPT** cells at this high current density, surpassing all other reported Al-organic batteries.^{40,56} The charge/discharge voltage profiles at 10 C rate (Fig. 2d) show two plateaus, representing the two well-defined redox processes of each PT unit with average discharge potentials of 1.48 and 0.74 V vs. Al|Al³⁺ (for differential capacity plots see Figure S26). Such flat charge/discharge plateaus are rarely observed in Al-organic batteries using p-type PEMs, in particular at such high current densities,^{40,41} and highlight the excellent suitability of **X-PVMPT**, if paired with EMIm-chloroaluminate as electrolyte, as PEM for AIBs.

Hence, herein we report the first reversible two-electron redox process for a PT-based battery electrode material, probably enabled by the ionic liquid electrolyte. Further, regarding the three combined parameters discharge voltage, specific capacity and capacity retention at fast C-rates, the **X-PVMPT**-electrodes reported herein outperform all other known organic PEMs in AIBs.³⁰ The redox processes are well distinguishable with a small voltage hysteresis between charge and discharge, even at high C-rates, advancing this system over other organic PEMs for AIBs.

Charge storage mechanism

A closer look at the charge/discharge profiles in Fig. 2d shows that the plateau at lower potential (average 0.74 V vs. Al|Al³⁺) favourably contributes only to a smaller amount of the specific capacity than the plateau at higher potential (average 1.48 V vs. Al|Al³⁺). Hence a larger amount of charge can be stored in the **X-PVMPT** electrodes at the higher potential than at the lower potential, which indicates that not all PT units partake in both redox processes **A** to **C** and **C** to **D** (see Fig. 1). To shed light into this cycling behaviour we performed constant current cycling measurements at 0.5 C rate (Fig. 3a) and investigated both charged and discharged electrodes using scanning electron microscopy (SEM) measurements combined with energy-dispersive X-ray (EDX) analyses (Fig. 3b). These measurements provide insight into the presence of chloroaluminate anions within the positive electrode in the different states of charge.

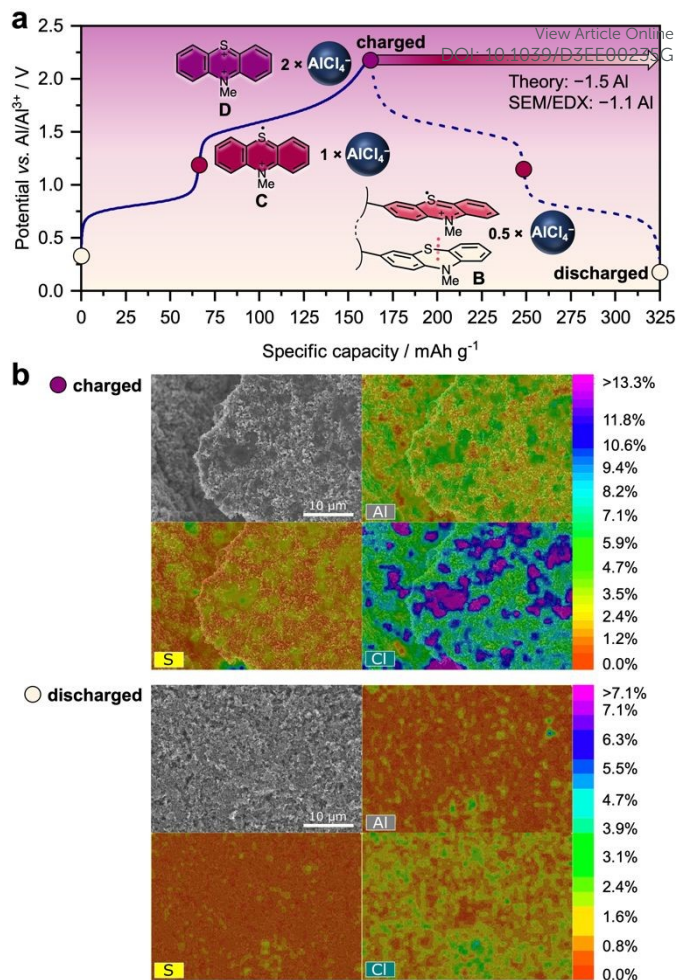


Fig. 3 | Charge/discharge mechanism of Al/**X-PVMPT** batteries. a, Charge/discharge profiles (at 0.5 C rate, after 50 cycles of pre-conditioning) with correlated oxidation states of the PT units and required [AlCl₄]⁻ ions for counterbalancing of charges (assuming that [AlCl₄]⁻ is the predominant inserting chloroaluminate ion based on its smaller size than [Al₂Cl₇]⁻)⁵⁴. b, SEM images of **X-PVMPT** electrodes in the charged (2.2 V vs. Al|Al³⁺) and discharged (to 0.3 V vs. Al|Al³⁺) state with atomic concentration heat map overlays based on EDX spectroscopy.

To remove additional electrolyte on the surface of the electrodes, the electrodes were carefully rinsed with *o*-difluorobenzene before the SEM/EDX measurements, nevertheless some electrolyte residuals cannot be fully excluded, hence quantification of Al/S ratio is not a quantitative representation of the state of charge (SOC) and should not be over interpreted. During the constant current cycling measurement at 0.5 C rate shown in Fig. 3a (51st cycle at 0.5 C rate), the plateaus during charge are centred at 0.81 and 1.65 V vs. Al|Al³⁺ (slightly differing from the potentials obtained at 10 C rate in Fig. 2d) and correspond to specific charge capacities of 66 mAh g⁻¹ and 98 mAh g⁻¹, respectively, in sum 164 mAh g⁻¹ for the complete charge cycle. Assuming that charge and discharge occur between oxidation states **B** and **D** (Fig. 1a), two equivalents of chloroaluminate anions ([AlCl₄]⁻/[Al₂Cl₇]⁻) are required in the fully charged state **D** of **X-PVMPT** to balance two positive charges on each PT unit, while 0.5 equivalents remain in the discharged state **B** (see also Fig. 3a).



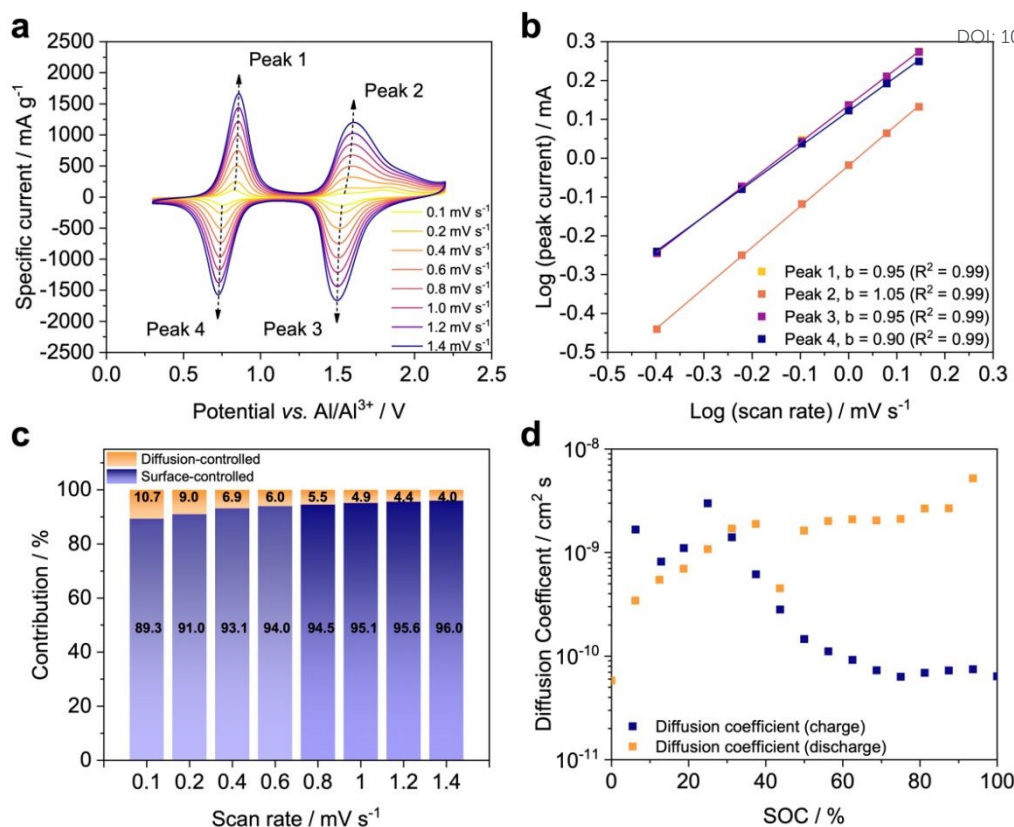


Fig. 4 | Electrochemical kinetics of Al/X-PVMPT batteries. a, CVs at various scan rates. b, Logarithmic plots of peak current vs. scan rate. c, Diffusion- and surface-controlled fractions of the redox reaction. d, Diffusion coefficients for $[\text{AlCl}_4]^-$ from GITT measurements (0.5 C rate, SOC = state of charge).

SEM/EDX spectra of the charged electrode show that significant amounts of Al and Cl are indeed present (Fig. 3b). Their localization correlates well with that of the sulphur atoms from the PT units, indicating their role as charge-stabilizing counter anions. In the discharged electrode, on the other hand, the Al and Cl concentrations are decreased, but both elements are still present. A quantification shows that the ratio of Al/S changes from 3.5 to 2.4 during discharge. Assuming that $[\text{AlCl}_4]^-$ is the predominant inserting chloroaluminate ion based on its smaller size than $[\text{Al}_2\text{Cl}_7]^-$,⁵⁴ this would correspond to a loss of 1.1 $[\text{AlCl}_4]^-$ ion equivalents relative to each PT unit in X-PVMPT. This correlates well with the expected value of 1.5 $[\text{AlCl}_4]^-$ ions, based on the observed specific discharge capacity of 164 mAh g^{-1} . This corresponds to a 74% utilization of the theoretical specific capacity for a 2-electron oxidation of each PT unit (221 mAh g^{-1}) and cycling between oxidation states **B** and **D** of X-PVMPT. Hence, the polymer is not reduced back to its neutral state during discharge, but retains some $[\text{AlCl}_4]^-$ (or $[\text{Al}_2\text{Cl}_7]^-$) ions in the discharged state, as expected for oxidation state **B**. The additional amounts of Al and Cl present in the electrode in both the charged and discharged form might be due to a solid-electrolyte interphase (SEI) layer, which formed in the initial cycles, as also observed by Nann and coworkers.⁶¹ Further, due to an excess of electrolyte employed, certain amounts of electrolyte with chloroaluminate ions might also still be present in the discharged electrode.

To further shed light into the charge storage mechanism of the Al/X-PVMPT batteries, we performed electrochemical kinetics studies. Evaluation of scan-rate dependent CVs allows to differentiate between diffusion- and surface-controlled redox processes. The scan-rate dependent CVs of X-PVMPT electrodes are plotted in Fig. 4a and show an increase of the anodic (Peaks 1 and 2) and cathodic (Peaks 3 and 4) peak currents with the scan rate. We use the known relationship between the peak current i and the scan rate v

$$i = kv^b \quad (\text{Eq. 1}),$$

with k and b being adjustable parameters.⁶² Here, a b value of 0.5 indicates a diffusion-controlled redox process, while a b value of 1 results from a surface-controlled redox reaction without diffusion limitation.^{31,62} A plot of $\log(i)$ vs. $\log(v)$, as shown in Fig. 4b, provided b -values of 0.90–1.05, indicating that the X-PVMPT electrodes' reaction is mainly dominated by surface-controlled process with no or minor diffusion limitation.

The surface-controlled process contribution was further investigated using Eq. 2 proposed by Kim et al..⁶³

$$I_{\text{tot}}(V) = k_1v + k_2v^{0.5} \quad (\text{Eq. 2})$$

k_1v corresponds to the surface-controlled current (proportional to the scan rate v) and $k_2v^{0.5}$ to the diffusion-controlled current. Rearranging the equation and linear fitting (see ESI) provides the k_1 and k_2 values, and the contributions from diffusion- and



surface-controlled processes can be derived as a function of potential (Figure S33). Fig. 4c shows that in the **X-PVMPT** electrodes the redox processes are surface-controlled by 89–96% at scan rates between 0.1–1.4 mV s⁻¹. This can be rationalized from the morphology of the electrodes, where the **X-PVMPT** is homogeneously dispersed with the conductive carbon additive (see SEM images in ESI). This leads to a close contact and – due to the porosity of the conductive carbon – short ion diffusion lengths between the electrolyte and the redox centres. The redox reactions take place near the surface of the positive electrode, and the rate of the electrochemical process is only slightly limited by the rate at which ions can diffuse to the redox units.

Further, the small size and non-coordinating nature of the [AlCl₄]⁻ counterions enable their fast diffusion within the positive electrode material, see also the diffusion coefficients plotted in Fig. 4d.

Hence, ion diffusion does take place close to the redox sites, as clearly visible from the shapes of the CVs in Fig. 4a and it is not a limiting factor. The amorphous morphology of the cross-linked **X-PVMPT** also contributes, which can increase the available space for ions to move and enhance the ionic conductivity, resulting in minor diffusion limitations, as discussed for other p-type network polymer in the literature.⁶⁴ This observation explains the excellent rate capability of the Al/**X-PVMPT** batteries, as the redox reactions in the positive electrode have no diffusion limitation.

We further evaluated the kinetics using the galvanostatic intermittent titration technique (GITT) (Figure S34). The measurement was performed after a pre-conditioning step of 50 cycles at 0.5 C. The GITT protocol consisted of alternating 6 min long constant current pulses at 0.5 C and rest steps of 1 h to allow for relaxation of the system. During charge, the insertion of the first [AlCl₄]⁻ ion (SOC below 50%) has a relatively fast kinetics with a diffusion coefficient *D* on the order of 10⁻⁹ cm² s⁻¹, while that of the second [AlCl₄]⁻ ion (SOC 50–100%) is associated with a smaller diffusion coefficient of ca. 10⁻¹⁰–10⁻¹¹ cm² s⁻¹ (Fig. 4d). In the discharge, the first [AlCl₄]⁻ ion deinserts quickly with *D* ≈ 10⁻⁹ cm² s⁻¹ (SOC 100–50%), and the second ion slightly slower with *D* ≈ 10⁻⁹–10⁻¹⁰ cm² s⁻¹ (SOC below 50%). The magnitude of these diffusion coefficients clearly indicates diffusion of the ions within the amorphous polymer phase. They are in a similar range as those reported for Al-graphite batteries, which lie in the order of *D* ≈ 10⁻⁸–10⁻⁹ cm² s⁻¹.⁶⁵ In conjunction with the strongly surface-controlled process they contribute to high rate capability of the **X-PVMPT** electrodes.

Conclusions

In summary, we have investigated cross-linked poly(3-vinyl-*N*-methylphenothiazine) (**X-PVMPT**) as organic positive electrode materials for insertion of [AlCl₄]⁻ ions in rechargeable Al batteries with an EMIm chloroaluminate electrolyte. Unprecedented for phenothiazine-based battery electrode materials, both redox processes of each phenothiazine unit could be used with this electrolyte and delivered experimental

specific capacities of up to 167 mAh g⁻¹. This well exceeds that of graphite in Al-graphite batteries, favourably further paired with an excellent cyclability and rate capability. Hence, 5,000 cycles at 10 C rate proceeded with 88% capacity retention, outperforming all other organic electrode materials for Al batteries. At the high current density of 4.4 A g⁻¹, the **X-PVMPT**-electrodes delivered a record specific discharge capacity of 136 mAh g⁻¹. Kinetic mechanistic investigations confirmed the reversible [AlCl₄]⁻ ion insertion during charge and showed that this process is not diffusion-limited, accounting for the excellent rate capability of the electrodes. Our study constitutes a major advance in the development of rechargeable Al batteries and will initiate further explorations of organic redox polymers as positive electrode materials together with ionic liquid-based electrolytes in such cells, paving the way towards more sustainable energy storage solutions.

Experimental

Materials and electrode preparation: The crosslinked **X-PVMPT** polymer with 10 mol% of crosslinker was synthesized using the same procedure as previously reported.⁴⁶ Its thermal analysis data can be found in Figures S11 and S12. Composite electrodes were prepared using 50 wt% **X-PVMPT**, 45 wt% carbon black (Acetylene Black, ALFA AESAR, 100% compressed, 99.9+%, 75 m² g⁻¹, bulk density 170–230 g l⁻¹) and 5 wt% PVdF (Kynar® HSV 900, ARKEMA). The components were mixed and dispersed in *N*-methyl-2-pyrrolidone (NMP, Acroseal®, THERMO SCIENTIFIC, 99.5%, stored over molecular sieves), using a planetary centrifugal mixer (ARM 310, THINKY MIXER). The electrode formulation was then cast onto molybdenum disks as current collectors (thickness: 1 mm, diameter: 12 mm, 99.9%, GOODFELLOW). The resulting coated disks were dried at ambient pressure for 12 h at 60 °C in a drying oven, then *in vacuo* (10⁻³ mbar, 60 °C, 24 h). The active material (**X-PVMPT**) mass loadings of the electrodes lay between 1.2–1.7 mg cm⁻².

Cell assembly: Electrochemical experiments were performed using a perfluoroalkoxy (PFA)-based *Swagelok*® three electrode cell setup (Figure S13). All cells were assembled in an Ar-filled Glovebox with H₂O and O₂ levels <0.1 ppm. The fabricated **X-PVMPT**-based electrodes were used as working electrodes (WE, diameter: 12 mm). Polished aluminium disks (CE, thickness: 1 mm, diameter: 12 mm, 99.999%, GOODFELLOW) were used as counter electrodes, and polished aluminium wire (RE, diameter: 1 mm, 99.999%, GOODFELLOW) as reference electrodes. Glass fibre separators (diameter: 13 mm, GF/D, *Whatman*™, CYTIVA) were placed between the WE and RE and between the RE and CE and soaked with 100 μL of electrolyte (AlCl₃ (99.999%, SIGMA ALDRICH): [EMIm]Cl (>98%, IOLITEC), 1.5 : 1.0).

Electrochemical measurements: Cyclic voltammetry and constant current measurements were performed on a MPG-2 battery testing system (BIOLOGIC SCIENCE INSTRUMENTS), after a constant current pre-cycling/conditioning step of 50 cycles at 0.5 C.

SEM/EDX: Scanning electron microscopy characterization was performed with a Hitachi field emission gun scanning electron microscope (FEG-SEM) SU8220 operated at 6 kV acceleration



voltage. EDX measurements were performed with the same acceleration voltage at a working distance of roughly 16 mm and recorded with a Bruker X-Flash detector. The software used for the data evaluation was Bruker esprit 2.5.1.221.

Author Contributions

B.E., I.K. and G.S. designed the concept of this project. B.E. and I.K. directed the research. G.S. performed the synthesis of **X-PVMPT**, all cell fabrication, electrochemical and kinetics measurements. A.S. conducted the experiments using additives for the ionic liquid electrolyte. A.F. and J.B. designed, and J.B. and G.S. performed the SEM/EDX experiments. M.S. performed the DFT calculations, coached by I.K. B.E. and G.S. wrote the manuscript. All authors discussed the results and commented on the manuscript.

Conflicts of interest

There are no conflicts to declare.

Acknowledgements

This work contributes to the research performed at CELEST (Center for Electrochemical Energy Storage Ulm-Karlsruhe) and was funded by the German Research Foundation (DFG) under Project ID 390874152 (POLiS Cluster of Excellence, EXC 2154) and 441215516 (SPP 2248 – Polymer-based batteries). Financial support through the German Federal Environmental Foundation (DBU, graduate fellowship for G.S.) is gratefully acknowledged as well as financial support from the Deutsche Forschungsgemeinschaft (DFG, German Research Foundation) under Germany's Excellence Strategy — EXC-2193/1 — 390951807 (livMatS Cluster of Excellence) and through grant no INST 40/575-1 FUGG (JUSTUS 2 cluster), the Eva Maria Stihl Stiftung in the project Saltus! and the state of Baden-Württemberg through bwHPC.

Notes and references

§ Including the masses of active materials and electrolytes

- 1 F. Wu, J. Maier and Y. Yu, *Chem. Soc. Rev.*, 2020, **49**, 1569–1614.
- 2 T. Kim, W. Song, D.-Y. Son, L. K. Ono and Y. Qi, *J. Mater. Chem. A*, 2019, **7**, 2942–2964.
- 3 J. Li, Z. Zhu, Y. Huang, F. Wang and M.-S. (Jie T. Balogun, *Mater. Today Energy*, 2022, **26**, 101001.
- 4 Y. Huang, H. Yang, T. Xiong, D. Adekoya, W. Qiu, Z. Wang, S. Zhang and M.-S. Balogun, *Energy Storage Mater.*, 2020, **25**, 41–51.
- 5 X. Yao, C. Li, R. Xiao, J. Li, H. Yang, J. Deng and M. -Sadee. Balogun, *Small*, 2022, **18**, 2204534.
- 6 Y. Tian, G. Zeng, A. Rutt, T. Shi, H. Kim, J. Wang, J. Koettgen, Y. Sun, B. Ouyang, T. Chen, Z. Lun, Z. Rong, K. Persson and G. Ceder, *Chem. Rev.*, 2021, **121**, 1623–1669.

- 7 Y. Liang, H. Dong, D. Aurbach and Y. Yao, *Nat. Energy*, 2020, **5**, 646–656. DOI: 10.1039/D3EE00235G
- 8 Committee TGAR, *Global aluminium recycling : A cornerstone of sustainable development*, 2009.
- 9 G. A. Elia, K. Marquardt, K. Hoepfner, S. Fantini, R. Lin, E. Knipping, W. Peters, J.-F. Drillet, S. Passerini and R. Hahn, *Adv. Mater.*, 2016, **28**, 7564–7579.
- 10 H. Chen, H. Xu, B. Zheng, S. Wang, T. Huang, F. Guo, W. Gao and C. Gao, *ACS Appl. Mater. Interfaces*, 2017, **9**, 22628–22634.
- 11 M. Galiński, A. Lewandowski and I. Stępnik, *Electrochim. Acta*, 2006, **51**, 5567–5580.
- 12 B. Craig, T. Schoetz, A. Cruden and C. Ponce de Leon, *Renew. Sustain. Energy Rev.*, 2020, **133**, 110100.
- 13 H. Yang, H. Li, J. Li, Z. Sun, K. He, H. Cheng and F. Li, *Angew. Chemie Int. Ed.*, 2019, **58**, 11978–11996.
- 14 T. Leisegang, F. Meutzner, M. Zschornak, W. Münchgesang, R. Schmid, T. Nestler, R. A. Eremin, A. A. Kabanov, V. A. Blatov and D. C. Meyer, *Front. Chem.*, 2019, **7**, 1–21.
- 15 Y. Zhang, S. Liu, Y. Ji, J. Ma and H. Yu, *Adv. Mater.*, 2018, **30**, 1706310.
- 16 F. Wu, H. Yang, Y. Bai and C. Wu, *Adv. Mater.*, 2019, **31**, 1806510.
- 17 L. Zhou, Z. Zhang, L. Cui, F. Xiong, Q. An, Z. Zhou, X.-F. Yu, P. K. Chu and K. Zhang, *Cell Reports Phys. Sci.*, 2021, **2**, 100354.
- 18 Y. Hu, D. Ye, B. Luo, H. Hu, X. Zhu, S. Wang, L. Li, S. Peng and L. Wang, *Adv. Mater.*, 2018, **30**, 1703824.
- 19 C. Legein, B. J. Morgan, F. Fayon, T. Koketsu, J. Ma, M. Body, V. Sarou-Kanian, X. Wei, M. Heggen, O. J. Borkiewicz, P. Strasser and D. Dambournet, *Angew. Chemie Int. Ed.*, 2020, **59**, 19247–19253.
- 20 X. Peng, Y. Xie, A. Baktash, J. Tang, T. Lin, X. Huang, Y. Hu, Z. Jia, D. J. Searles, Y. Yamauchi, L. Wang and B. Luo, *Angew. Chemie Int. Ed.*, DOI:10.1002/anie.202203646.
- 21 X. Han, S. Li, W. Song, N. Chen, H. Chen, S. Huang and S. Jiao, *Adv. Energy Mater.*, 2021, **11**, 2101446.
- 22 D.-J. Yoo, M. Heeney, F. Glöckhofer and J. W. Choi, *Nat. Commun.*, 2021, **12**, 2386.
- 23 J. Bitenc, N. Lindahl, A. Vizintin, M. E. Abdelhamid, R. Dominko and P. Johansson, *Energy Storage Mater.*, 2020, **24**, 379–383.
- 24 N. Lindahl, J. Bitenc, R. Dominko and P. Johansson, *Adv. Funct. Mater.*, 2020, **2004573**, 2004573.
- 25 X. Xiao, M. Wang, J. Tu, Y. Luo and S. Jiao, *ACS Sustain. Chem. Eng.*, 2019, **7**, 16200–16208.
- 26 G. A. Elia, I. Hasa, G. Greco, T. Diemant, K. Marquardt, K. Hoepfner, R. J. Behm, A. Hoell, S. Passerini and R. Hahn, *J. Mater. Chem. A*, 2017, **5**, 9682–9690.
- 27 D.-Y. Y. Wang, C.-Y. Y. Wei, M.-C. C. Lin, C.-J. J. Pan, H.-L. L. Chou, H.-A. A. Chen, M. Gong, Y. Wu, C. Yuan, M. Angell, Y.-J. J. Hsieh, Y.-H. H. Chen, C.-Y. Y. Wen, C.-C. C.-W. W. Chen, B.-J. J. Hwang, C.-C. C.-W. W. Chen and H. Dai, *Nat. Commun.*, 2017, **8**, 14283.
- 28 S. Wang, K. V. Kravchyk, F. Krumeich and M. V. Kovalenko, *ACS Appl. Mater. Interfaces*, 2017, **9**, 28478–28485.
- 29 K. V. Kravchyk, S. Wang, L. Piveteau and M. V. Kovalenko,



- Chem. Mater.*, 2017, **29**, 4484–4492.
- 30 Z. Yang, F. Wang, P. Meng, J. Luo and C. Fu, *Energy Storage Mater.*, 2022, **51**, 63–79.
- 31 C. N. Gannett, L. Melecio-Zambrano, M. J. Theibault, B. M. Peterson, B. P. Fors and H. D. Abruña, *Mater. Reports Energy*, 2021, **1**, 100008.
- 32 B. Esser, F. Dolhem, M. Becuwe, P. Poizot, A. Vlad and D. Brandell, *J. Power Sources*, 2021, **482**, 228814.
- 33 Y. Lu and J. Chen, *Nat. Rev. Chem.*, 2020, **4**, 127–142.
- 34 J. Xie and Q. Zhang, *Small*, 2019, **15**, 1805061.
- 35 H. Ye and Y. Li, *Energy & Fuels*, 2021, **35**, 7624–7636.
- 36 K. Qin, J. Huang, K. Holguin and C. Luo, *Energy Environ. Sci.*, 2020, **13**, 3950–3992.
- 37 N. S. Hudak, *J. Phys. Chem. C*, 2014, **118**, 5203–5215.
- 38 M. Walter, K. V. Kravchyk, C. Böfer, R. Widmer and M. V. Kovalenko, *Adv. Mater.*, 2018, **30**, 1705644.
- 39 T. Schoetz, B. Craig, C. Ponce de Leon, A. Bund, M. Ueda and C. T. J. Low, *J. Energy Storage*, 2020, **28**, 101176.
- 40 G. Wang, E. Dmitrieva, B. Kohn, U. Scheler, Y. Liu, V. Tkachova, L. Yang, Y. Fu, J. Ma, P. Zhang, F. Wang, J. Ge and X. Feng, *Angew. Chemie Int. Ed.*, , DOI:10.1002/anie.202116194.
- 41 Y. Kong, C. Tang, C. Lei, A. K. Nanjundan, S. Chen, N. Ahmed, D. Rakov, A. Du, X. Huang and C. Yu, *Nano Energy*, 2022, **102**, 107727.
- 42 W. Ma, L. Luo, X. Huang, P. Dong, Y. Chen, C. Zhang, F. Huang, J. Jiang and Y. Cao, *Adv. Energy Mater.*, 2023, **13**, 2203253.
- 43 B. Esser, *Org. Mater.*, 2019, **01**, 063–070.
- 44 V. Perner, D. Diddens, F. Otteny, V. Küpers, P. Bieker, B. Esser, M. Winter and M. Kolek, *ACS Appl. Mater. Interfaces*, 2021, **13**, 12442–12453.
- 45 F. Otteny, G. Studer, M. Kolek, P. Bieker, M. Winter and B. Esser, *ChemSusChem*, 2020, **13**, 2232–2238.
- 46 F. Otteny, M. Kolek, J. Becking, M. Winter, P. Bieker and B. Esser, *Adv. Energy Mater.*, 2018, **8**, 1802151.
- 47 M. Kolek, F. Otteny, P. Schmidt, C. Mück-Lichtenfeld, C. Einholz, J. Becking, E. Schleicher, M. Winter, P. M. Bieker and B. Esser, *Energy Environ. Sci.*, 2017, **10**, 2334–2341.
- 48 P. Acker, J. S. Wössner, G. Desmaizieres and B. Esser, *ACS Sustain. Chem. Eng.*, 2022, **10**, 3236–3244.
- 49 F. Otteny, G. Desmaizieres and B. Esser, in *Redox Polymers for Energy and Nanomedicine*, eds. N. Casado and D. Mecerreyes, Royal Society of Chemistry, 2020, pp. 166–197.
- 50 Z. Yang, X. Huang, P. Meng, M. Jiang, Y. Wang, Z. Yao, J. Zhang, B. Sun and C. Fu, *Angew. Chemie Int. Ed.*, , DOI:10.1002/anie.202216797.
- 51 C. Ferrara, V. Dall'Asta, V. Berbenni, E. Quartarone and P. Mustarelli, *J. Phys. Chem. C*, 2017, **121**, 26607–26614.
- 52 P. R. Gifford and J. B. Palmisano, *J. Electrochem. Soc.*, 1988, **135**, 650–654.
- 53 P. K. Lai and M. Skyllas-Kazacos, *J. Electroanal. Chem. Interfacial Electrochem.*, 1988, **248**, 431–440.
- 54 W. R. Carper, C. E. Keller, N. A. Evangelos and M. E. Zandler, *Main Gr. Chem.*, 1996, **1**, 257–263.
- 55 Y. Park, D. Lee, J. Kim, G. Lee and Y. Tak, *Phys. Chem. Chem. Phys.*, 2020, **22**, 27525–27528.
- D. J. Kim, D.-J. Yoo, M. T. Otle, A. Prokofjev, C. Pezzato, M. Owczarek, S. J. Lee, J. W. Choi and J. F. Stoddart, *Nat. Energy*, 2019, **4**, 51–59.
- M. Kolek, F. Otteny, J. Becking, M. Winter, B. Esser and P. Bieker, *Chem. Mater.*, 2018, **30**, 6307–6317.
- E. Faegh, B. Ng, D. Hayman and W. E. Mustain, *Nat. Energy*, 2021, **6**, 21–29.
- H. Chen, H. Xu, S. Wang, T. Huang, J. Xi, S. Cai, F. Guo, Z. Xu, W. Gao and C. Gao, *Sci. Adv.*, , DOI:10.1126/sciadv.aao7233.
- M.-C. Lin, M. Gong, B. Lu, Y. Wu, D.-Y. Wang, M. Guan, M. Angell, C. Chen, J. Yang, B.-J. Hwang and H. Dai, *Nature*, 2015, **520**, 324–328.
- N. Canever, F. R. Hughson and T. Nann, *ACS Appl. Energy Mater.*, 2020, **3**, 3673–3683.
- H. Lindström, S. Södergren, A. Solbrand, H. Rensmo, J. Hjelm, A. Hagfeldt and S.-E. Lindquist, *J. Phys. Chem. B*, 1997, **101**, 7717–7722.
- H.-S. Kim, J. B. Cook, H. Lin, J. S. Ko, S. H. Tolbert, V. Ozolins and B. Dunn, *Nat. Mater.*, 2017, **16**, 454–460.
- B. M. Peterson, C. N. Gannett, L. Melecio-Zambrano, B. P. Fors and H. Abruña, *ACS Appl. Mater. Interfaces*, 2021, **13**, 7135–7141.
- D. Han, M. Cao, N. Li, D. She, W. Song, H. Chen, S. Jiao and D. Fang, *Chinese J. Chem.*, 2021, **39**, 157–164.

View Article Online
DOI: 10.1039/D2EE00235G